



# CHORUS

This is the accepted manuscript made available via CHORUS. The article has been published as:

## Zinc-blende to rocksalt transition in SiC in a laser-heated diamond-anvil cell

Kierstin Daviau and Kanani K. M. Lee

Phys. Rev. B **95**, 134108 — Published 18 April 2017

DOI: [10.1103/PhysRevB.95.134108](https://doi.org/10.1103/PhysRevB.95.134108)

# Zinc-blende to Rock-salt transition in SiC in a Laser-Heated Diamond-Anvil Cell

Kierstin Daviau<sup>1,\*</sup> and Kanani K. M. Lee<sup>1</sup>

<sup>1</sup>Department of Geology & Geophysics, Yale University, New Haven, CT 06511

\* corresponding author; [kierstin.daviau@yale.edu](mailto:kierstin.daviau@yale.edu)

We explore the stability of the ambient pressure zinc-blende polymorph (B3) structure of silicon carbide (SiC) at high pressures and temperatures where it transforms to the rock-salt (B1) structure. We find that the transition occurs  $\sim 40$  GPa lower than previously measured when heated to moderately high temperatures. A lower transition pressure is consistent with the transition pressures predicted in numerous ab initio computations. We find a large volume decrease across the transition of  $\sim 17\%$ , with the volume drop increasing at higher formation pressures, suggesting this transition is volume driven yielding a nearly pressure-independent Clapeyron slope. Such a dramatic density increase occurring at pressure is important to consider in applications where SiC is exposed to extreme conditions, such as in industrial applications or planetary interiors.

## I. INTRODUCTION

SiC is an attractive material due to its high melting point, high thermal conductivity, high strength, and relatively low density. The stability of SiC at extreme conditions is important to understand as we further develop its use in the nuclear, aerospace, and energy industries. SiC is also a candidate material to make up the interior of carbon-rich exoplanets [1]. Understanding the structure and density of these planets is dependent on our understanding of the high P-T behavior of SiC.

The high-pressure transition from the zinc-blende (B3) to the rock-salt (B1) structure in SiC has been explored extensively in computations [2-9]. In comparison, experimental studies are sparse [10-14]: only one static [11] study has explored high enough pressures ( $\sim 100$  GPa) to observe the transition directly at room temperature and finds a large reduction in volume at the transition of 20.3%. Another study on the hexagonal 6H form of SiC under comparable shock conditions also sees indication of a phase transition based on a large increase in the density, however the crystal structure was not determined [10]. Additional studies have observed a softening in Raman modes while at high-pressure conditions for B3 SiC [14] and 6H SiC [12]. Such softening was inferred to be an indication of a coming transition and provides indirect constraints on the phase boundary. Experimentally, no studies have directly considered the temperature effects on the B3 to B1 transition in SiC and no experimental equation of state has been attempted despite numerous predictions.

Using the laser-heated diamond-anvil cell (LHDAC) combined with in situ x-ray diffraction (XRD), we investigate the B3 to B1 transition in SiC. We find that the addition of

temperature lowers the transition pressure considerably. We explore the transformation kinetics across a pressure range of 50 to 70 GPa while laser heating up to temperatures of  $\sim 2250$  K. Our experiments put tighter constraints on the bounds of B3 SiC stability. Across the B3 to B1 transition, we find a dramatic increase in density that is consistent with both computations and previous experiment. Such a dramatic density change is important to consider in both industrial and planetary applications.

## II. METHODS

Our samples consist of B3 SiC powder purchased from Alfa Aesar (product #14165 and lot #121X047). Using 200 or 300  $\mu\text{m}$  culet diamonds, we compressed the SiC powder into an 80 or 125  $\mu\text{m}$  drilled hole in a pre-indented rhenium gasket using the double-sided stepped anvil technique [15]. We gas loaded neon (Ne) [16] as a pressure medium and as thermal insulation (Fig.1). All XRD measurements were completed at the HPCAT-IDB beamline at the Advanced Photon Source [17] at Argonne National Lab ( $\lambda=0.406626$   $\text{\AA}$ ).

We determined pressure before and after laser heating by the Ne equation of state (EOS) [18] with the corrections recommended in [19], as well as by the diamond edge Raman shift [20]. While laser heating, we could not measure simultaneous Raman spectra and so depend on the Ne EOS for pressure determination. For all of our pressure measurements we used the room-temperature Ne equation of state without thermal correction, as we expect the Ne to remain relatively cool throughout laser heating. We increased pressure on our samples prior to heating. Heating was performed systematically from both sides while numerous temperature measurements and diffraction patterns were taken. After several minutes at a single power, we quenched the laser, took an XRD pattern at room temperature, and then increased the laser power to achieve a higher temperature (Fig. 2). We performed three separate experimental runs at different pressure conditions; details are listed in Table I.

Upon completion of the laser heating, the sample was decompressed slowly at room temperature, with diffraction taken both on and off the heated spot for comparison at each pressure (Fig. 3). We observed dramatic hysteresis effects on decompression for Y02\_042016, but much less hysteresis upon decompressing Y04\_111716. In both cases the B3 SiC eventually quenched to its original zero pressure volume. The B1 phase did not quench.

## III. RESULTS

Prior to laser heating, all of the XRD diffraction peaks were identified as either Ne, B3 SiC and a few weak peaks of 6H SiC. Upon laser heating, we observe a phase change in B3 SiC to the B1 structure in experiment Y02\_042016 and Y04\_111716. Figure 2 shows the formation of B1 SiC as measured by XRD in Y02\_042016. In this experiment, we observed rapidly intensifying B1 peaks while maintaining a temperature measured between 1700-1800 K. We

find four to five peaks corresponding to the B1 phase, as compared to the three peaks previously measured [11]. Table 2 lists the d-spacing and the hkl of each of the reflection peaks for the observed B1 SiC, as well as for those found previously [11]. Our measured values match the calculated d-spacings to within 0.001 Å and follow the general trend of both calculated and previously observed intensities. In Y02\_042016, at 62 GPa, the spacing corresponds to a lattice parameter  $a = 3.831 (\pm 0.001)$  Å, corresponding to a volume of  $56.251 (\pm 0.044)$  Å<sup>3</sup>. For the B3 SiC in the same XRD pattern, the d-spacing corresponds to a lattice parameter of  $a = 4.06 (\pm 0.001)$  Å ( $V = 67.36 (\pm 0.065)$  Å<sup>3</sup>), resulting in a difference in volume  $\Delta V$  across the transition of 16.5%. We observed formation of the same phase in experiment Y04\_111716 at 67 GPa with a lattice parameter of  $a = 3.812 (\pm 0.001)$  Å, corresponding to a volume of  $55.405 (\pm 0.030)$  Å<sup>3</sup>, and a volume drop of 17.4%. In experiment Y03\_111716, at 47 GPa, we saw no indication of the B1 phase while heating to temperatures up to  $\sim 2250$  K.

Several previous studies have explored the possibility of transition structures during the B3 to B1 transition in SiC. LCAO-DFT least-enthalpy calculations [2] show that as B3 SiC transforms to B1 SiC, it first forms an orthorhombic structure with *Pmm2* symmetry as part of the transformation pathway. More recent ab initio computations [4] instead predict that a tetragonal *I4m2* phase forms at the onset of symmetry breaking in B3 SiC at the start of the transformation to B1. As the transformation continues, the same calculations show that SiC forms an orthorhombic phase with *Imm2* symmetry. We find no evidence in our measurements for any of the transition structures predicted in [4] or [2].

We do observe a dramatic change in optical absorption upon heating, as can be seen in the inset of Fig. 2. Before heating, B3 SiC is mostly opaque. The rim between the heated and unheated portion of the sample is significantly more transparent, however, while the central heated portion is opaque. We note that there was no evidence of damage to the anvils upon unloading these samples. The absorption changes in the SiC remain after quenching, leading us to infer that they are not directly related to the B1 phase, but rather to another change brought about by high pressures and/or high temperatures. A shift towards becoming more transparent to visible light has been observed previously in 6H SiC at high-pressures and room temperature [12]. It has been suggested [21] that changes in the microstructure of B3 SiC corresponds to changes in the opacity, with opaque SiC containing more defects than transparent SiC. It is possible that some of the absorption changes we observe during heating are due to the annealing of defects, although this may not fully explain the changes in opacity. Current efforts by our group are underway to better characterize and explain the absorption changes in SiC.

Selections of our decompression patterns from Y02\_042016 are shown in Fig. 3. There are two XRD patterns shown at each step upon decompression. One pattern corresponds to a spot in the sample 20  $\mu\text{m}$  from the heated location where there was no B3 to B1 transition, while the second pattern corresponds to a spot within the heated location where the B3 to B1 transition occurred. Ne diffraction in the unheated regions was also used to calculate pressure, although we observe a significant offset between the diamond edge Raman pressures and those determined by Ne diffraction as pressures are decreased. This may be due to uneven stresses

within the sample chamber [22]. For example, it is apparent from the shift in the B3 SiC reflections that the pressure felt by B3 SiC between the heated and unheated locations is different in each set of decompression patterns. The volume difference of B3 SiC between the two patterns is typically about a cubic angstrom, corresponding to a pressure difference along the B3 SiC EOS [19] of greater than 6 GPa in most cases. This pressure difference may be due to uneven stresses due to migration of the Ne pressure medium while heating.

Once the pressure dropped below  $\sim 52$  GPa, we saw a significant broadening and decreased intensity of the B1 peaks. They disappeared completely by 45 GPa confirming that the B1 structure does not quench and consistent with the previous study [11]. We find a significant amount of hysteresis in our decompression volumes in Y02\_042016, although the volumes of B3 and B1 track one another indicating that the trend is not specific to one structure, but is instead present throughout the sample chamber. Decompression of Y04\_111716 showed much less hysteresis and also saw the disappearance of B1 peaks at pressures below 40 GPa.

Our measured volumes of rock-salt SiC and that predicted via ab initio computations show general good agreement (Fig. 4, Table 2). We find that our lowest transition pressure matches nearly exactly that predicted by most computations and our change in volume across the transition is similar to that predicted. A variety of computational techniques have been utilized previously, resulting in the range of values found and listed in Table 3. The studies using density functional theory (DFT) find a transition pressure between 58 GPa [6] and 75 GPa [7], with the average transition pressure across five DFT studies being 65.8 GPa, albeit at 0 K. The differences in these studies is likely due to the approximations used; [5,7] use the local density approximation (LDA), while [6,8] use the generalized gradient approximation (GGA). The calculations in [8] were done using both a Perdew-Burke-Ernzerhof (PBE) and a Perdew-Burke-Ernzerhof for solids (PBEsol) GGA. Ab initio pseudopotentials were used in [3], resulting in a similar transition pressure of 66 GPa, while molecular dynamics (MD) were used in [9] yielding a much higher transition pressure of 140 GPa.

It was suggested in [11] that compression without heating may result in overestimating the transition pressure, possibly explaining why we see the same transition at  $\sim 40$  GPa lower when laser heating as compared to the previous compression experimental study. In B1 SiC synthesized at 62 GPa (Y02\_042016), we find a volume that is  $6.45 \text{ \AA}^3$  larger than that found by [11] at 100 GPa. For this  $\Delta V$ , the extra 38 GPa of compression to achieve the phase transition in [11] corresponds to a compression energy of  $\sim 0.191$  eV per atom. In our experiment, the 1800 K needed to achieve the phase transition corresponds to 0.155 eV. The same calculation for the B1 SiC formed in Y04\_111716 results in an additional compression energy in [11] of 0.140 eV per atom as compared to the 0.129 eV we input at 1500 K.

The small discrepancy between the energies can be accounted for by an offset in pressure due to different calibration standards or pressure gradients between the studies, as well as due to energy lost in [11] to additional deformation of the sample and/or gasket. A change in the transparency of samples during heating has also been identified as causing potentially significant errors in temperature determination due to wavelength-dependent absorption changes [23]. The

temperatures we present here have not been corrected for this effect, however, the temperature correction is likely minimal as SiC is surrounded by the transparent Ne pressure medium and the peak temperature is measured over a nearly fully opaque SiC. A higher actual temperature would increase our thermal energy input to that closer to the compression energy in [11].

By fitting a line to the P-T conditions of our formation data, as well as the previous data point from [11], we find a steep negative slope to the phase boundary of  $\sim -26.4 \pm 3.9$  MPa/K for the B3 to B1 phase transition. Errors come from the high and low temperature bounds on our double-sided laser heating measurements, as well as our inclusion of the previous data uncertainties. Using only our two measurements, we calculate this slope to be  $-19.4 \pm 3.2$  MPa/K. However, due to the strong kinetics involved in the B3 to B1 transition, the phase boundary found using the experimental data is not representative of the equilibrium transition conditions. It is likely that our experiments are overdriven with respect to the equilibrium pressure and temperature transition conditions, giving rise to an apparently very steep slope along the phase boundary. As the B3 to B1 transition is largely volume driven, with a very large volume collapse compared to the entropy change across the transition, we expect that the Clapeyron slope is much shallower than our experiments indicate. By following the model presented in [24] we approximate the Clapeyron slope for the B3 to B1 transition at equilibrium conditions. We find a much shallower, nearly pressure-independent phase boundary (Fig. 5). Details of the calculation are presented in the Supplemental Material [25]. Potentially large uncertainties come from a lack of data on the elastic parameters of B1 SiC at the transition conditions. We consider a change of  $\pm 30\%$  in the elastic parameters of B1 SiC relative to B3 SiC in order to explore how sensitive the Clapeyron slope is to relative changes in the parameters between the B1 and B3 phase. We find that either a slightly positive or slightly negative slope is possible with the currently available constraints (Fig. 5). The upper bound has a slope of 1.8 MPa/K while the lower bound has a slope of -0.7 MPa/K.

We find that the density jump across the B3 to B1 transition is 16.5% at 62 GPa and  $\sim 1800$  K, and 17.4% at 67 GPa and  $\sim 1500$  K (Table 2). The previous diamond cell study [11] found a density jump of 20.3% at 100 GPa and room temperature. From a planetary context, a large increase in the density of SiC will affect carbon planet interior structure and dynamics, as well as the high-pressure equation of state used to identify planet composition. SiC is less dense than silicate materials;  $\sim 3210$  kg/m<sup>3</sup> at room conditions as compared to Mg-silicate perovskite (i.e., bridgmanite [26]), where Mg-endmember MgSiO<sub>3</sub> has a room-conditions density of  $\sim 4100$  kg/m<sup>3</sup> [27]. This density difference has been used to identify potential carbon-rich exoplanets [28]. However, if SiC becomes  $\sim 17\%$  more dense at 60 GPa, the expected density of a carbon-rich planet will be greater than previously thought, nearly matching that of bridgmanite.

We model the mass-radius (M-R) relation of a planet for different interior compositions based on the procedure in [29] considering several different scenarios. We recreate the mass-radius curve for SiC planets using the equation of state for the B3 structure, as used in [28-30] for possible carbon planet identification. We also plot the mass-radius curve for a SiC planet using the B1 equation of state as determined in [31] for large carbon-rich bodies. For

comparison, we also reproduce the mass-radius relation for  $\text{MgSiO}_3$  bridgmanite, Fe and  $\text{H}_2\text{O}$  ice [29,30] (Fig. 6).

We find that the M-R curve for carbon-rich planets composed of B1 SiC and planets composed of bridgmanite are nearly identical. When the high pressure B3 to B1 phase change is taken into account, we cannot distinguish a SiC planet from a silicate one based on the M-R curve alone.

A density increase of this magnitude will also have an impact on the interior structure and dynamics of a body containing SiC. In the Earth, relatively small changes in density may result in dramatic topography, such as that found above the core-mantle boundary (e.g., [32]) The presence of such a dramatic density change mid-way through the mantle of a carbon planet will likely have an impact on convection and heat transport throughout the body.

#### IV. CONCLUSIONS

Our experiments indicate that the B3 to B1 transition in SiC is a kinetically hindered reaction and occurs at much lower pressures when hot than previously found experimentally. This transition pressure is consistent with most computations as well as being consistent with previous DAC experiments. In addition to this structural transition we also observe absorption changes from transparent to very opaque in the center of the heated area. Both the large volume change upon transition and the absorption changes upon heating may be important to consider in contexts where high pressures and temperatures are present, such as in planetary interiors or in industrial applications. We recommend that the B3 to B1 transition be taken into account when attempting to identify planets with a potentially carbon-rich interior. Our models indicate that once the transition is included, the bulk density of carbon-rich planets may not differ as extremely from silicate planets as previously deduced ([30], [28]). This calls into question our ability to distinguish carbon planets from silicate planets using bulk density measurements and further complicates the already non-unique nature of mass-radius curves for exoplanets.

#### ACKNOWLEDGEMENTS

We acknowledge support from the DOE through the Carnegie DOE Alliance Center (CDAC). We also thank Yue Meng and Ross Hrubiak for assistance at the HPCAT IDB beamline as well as Sergey Tkachev for gas loading with the system at GSECARS. This work was performed at HPCAT (Sector 16), Advanced Photon Source (APS), Argonne National Laboratory. HPCAT operations are supported by DOE-NNSA under Award No. DE-NA0001974 and DOE-BES under Award No. DE-FG02-99ER45775, with partial instrumentation funding by NSF. The Advanced Photon Source is a U.S. Department of Energy (DOE) Office of Science User Facility operated for the DOE Office of Science by Argonne National Laboratory under Contract No. DE-AC02-06CH11357. Use of the COMPRES-GSECARS gas loading system was supported by COMPRES under NSF Cooperative Agreement EAR 11-57758 and by GSECARS

through NSF grant EAR-1128799 and DOE grant DE-FG02-94ER14466. This research used resources of the Advanced Photon Source, a U.S. Department of Energy (DOE) Office of Science User Facility operated for the DOE Office of Science by Argonne National Laboratory under Contract No. DE-AC02-06CH11357.

- [1] M. J. Kuchner and S. Seager, arXiv preprint astro-ph/0504214 (2005).
- [2] M. Catti, Physical review letters **87**, 035504 (2001).
- [3] K. J. Chang and M. L. Cohen, Physical Review B **35**, 8196 (1987).
- [4] M. Durandurdu, Journal of Physics: Condensed Matter **16**, 4411 (2004).
- [5] K. Karch, F. Bechstedt, P. Pavone, and D. Strauch, Physical Review B **53**, 13400 (1996).
- [6] W. Lee and X. Yao, Computational Materials Science **106**, 76 (2015).
- [7] Y.-P. Lu, D.-W. He, J. Zhu, and X.-D. Yang, Physica B: Condensed Matter **403**, 3543 (2008).
- [8] M. S. Miao and W. R. L. Lambrecht, Physical Review B **68**, 092103 (2003).
- [9] F. Shimojo, I. Ebbsjö, R. K. Kalia, A. Nakano, J. P. Rino, and P. Vashishta, Physical review letters **84**, 3338 (2000).
- [10] T. Sekine and T. Kobayashi, Physical Review B **55**, 8034 (1997).
- [11] M. Yoshida, A. Onodera, M. Ueno, K. Takemura, and O. Shimomura, Physical Review B **48**, 10587 (1993).
- [12] J. Liu and Y. K. Vohra, Physical review letters **72**, 4105 (1994).
- [13] D. Olego, M. Cardona, and P. Vogl, Physical Review B **25**, 3878 (1982).
- [14] A. Debernardi, C. Ulrich, K. Syassen, and M. Cardona, Physical Review B **59**, 6774 (1999).
- [15] Z. Du, T. Gu, V. Dobrosavljevic, S. T. Weir, S. Falabella, and K. K. Lee, Review of Scientific Instruments **86**, 095103 (2015).
- [16] M. Rivers, V. B. Prakapenka, A. Kubo, C. Pullins, C. M. Holl, and S. D. Jacobsen, High Pressure Research **28**, 273 (2008).
- [17] Y. Meng, G. Shen, and H. Mao, Journal of Physics: Condensed Matter **18**, S1097 (2006).
- [18] Y. Fei, A. Ricolleau, M. Frank, K. Mibe, G. Shen, and V. Prakapenka, Proceedings of the National Academy of Sciences **104**, 9182 (2007).
- [19] K. K. Zhuravlev, A. F. Goncharov, S. N. Tkachev, P. Dera, and V. B. Prakapenka, Journal of Applied Physics **113**, 113503 (2013).
- [20] Y. Akahama and H. Kawamura, Journal of applied physics **96**, 3748 (2004).
- [21] Y. Kim, A. Zangvil, J. S. Goela, and R. L. Taylor, Journal of the American Ceramic Society **78**, 1571 (1995).
- [22] K. Glazyrin, N. Miyajima, J. S. Smith, and K. K. Lee, Journal of Geophysical Research: Solid Earth (2016).
- [23] J. Deng, Z. Du, L. R. Benedetti, and K. K. Lee, Journal of Applied Physics **121**, 025901 (2017).
- [24] X. Li and R. Jeanloz, Physical Review B **36**, 474 (1987).

- [25] See Supplemental Material at [URL will be inserted by publisher] for details of the calculation of the Clapeyron slope at equilibrium conditions.
- [26] O. Tschauner, C. Ma, J. R. Beckett, C. Prescher, V. B. Prakapenka, and G. R. Rossman, *Science* **346**, 1100 (2014).
- [27] B. B. Karki, R. M. Wentzcovitch, S. de Gironcoli, and S. Baroni, *Physical Review B* **62**, 14750 (2000).
- [28] N. Madhusudhan, K. K. M. Lee, and O. Mousis, *The Astrophysical Journal Letters* **759**, L40 (2012).
- [29] Y.-X. Gong and J.-L. Zhou, *Research in Astronomy and Astrophysics* **12**, 678 (2012).
- [30] S. Seager, M. Kuchner, C. Hier-Majumder, and B. Militzer, *The Astrophysical Journal* **669**, 1279 (2007).
- [31] H. F. Wilson and B. Militzer, *The Astrophysical Journal* **793**, 34 (2014).
- [32] E. J. Garnero, A. K. McNamara, and S.-H. Shim, *Nature Geoscience* (2016).
- [33] Q. Chen and B. Sundman, *Acta materialia* **49**, 947 (2001).

## FIGURE CAPTIONS

FIG. 1. Schematic of LHDAC sample setup.

FIG. 2. Formation of B1 SiC from B3 SiC during laser heating for Y02\_042016. Reflection peaks of Neon (Ne) and SiC in the rock-salt (B1) and zinc-blende (B3) structures are labeled with the appropriate hkl. Weak diffraction from 6H SiC is also observed and labeled with an asterisk. Diamond diffraction is labeled with a solid black diamond. (Inset) Optical image taken at pressure after heating. The visibly opaque region on the right-hand side corresponds to the heated location, while the more visibly transparent region surrounds the edge of the heated spot.

FIG. 3. A series of room-temperature XRD patterns taken on decompression on the heated area (solid curves) and 20  $\mu\text{m}$  away on the unheated area (dashed curves) for Y02\_042016. Reflections of B1, B3 and Ne are labeled. XRD peaks from diamond and the Re gasket as shown by diamond and star symbols, respectively. Pressures listed were determined from the room-temperature EOS of Ne [19].

FIG. 4. Pressure versus room-temperature volume for B3 and B1 SiC during synthesis and decompression for experiment runs Y02\_042016 (circles) and Y04\_111716 (squares). Solid symbols indicate synthesis conditions while open symbols indicate volumes measured on decompression. The room-temperature B3 volume for Y03\_111716 is shown as a solid triangle where no B1 was formed at high temperatures. Pressure is determined by Ne, while the pressure error bars show the range between Ne pressures and those determined by the Raman edge of diamond [20]. Errors in volume are smaller than the symbols ( $\sim 0.05 \text{ \AA}^3$ ). Previous DAC experimental result [11] for B1 volume is plotted as a solid black diamond. Selected EOSs as determined by ab initio computations for B1 [5-7] and an experimental EOS [19] for B3 are shown for comparison.

FIG. 5. Phase boundary between B3 and B1 SiC. The transition pressure and temperature are plotted for experimental runs Y02\_042016 (solid circle) and Y04\_111716 (solid square). As we

did not observe the B3 to B1 transition in Y03\_111716, the peak temperature condition (open triangle) is plotted for this experiment. The experimental phase boundary for the B3 to B1 transition between our two transition points is shown as a dashed line, while the upper and lower bounds for the calculated Clapeyron slope at equilibrium conditions [24,33] are shown as a shaded region for a 0 K transition pressure of 58 GPa [6].

FIG. 6. Modeled planet mass and radius (in Earth-mass and Earth-radii) for planet interiors composed entirely of the B3 SiC (dotted), B1 SiC (solid) in comparison with H<sub>2</sub>O ice (dashed), MgSiO<sub>3</sub> bridgmanite (dash-dot) and Fe (long dash-dot) [30].

FIG 1.

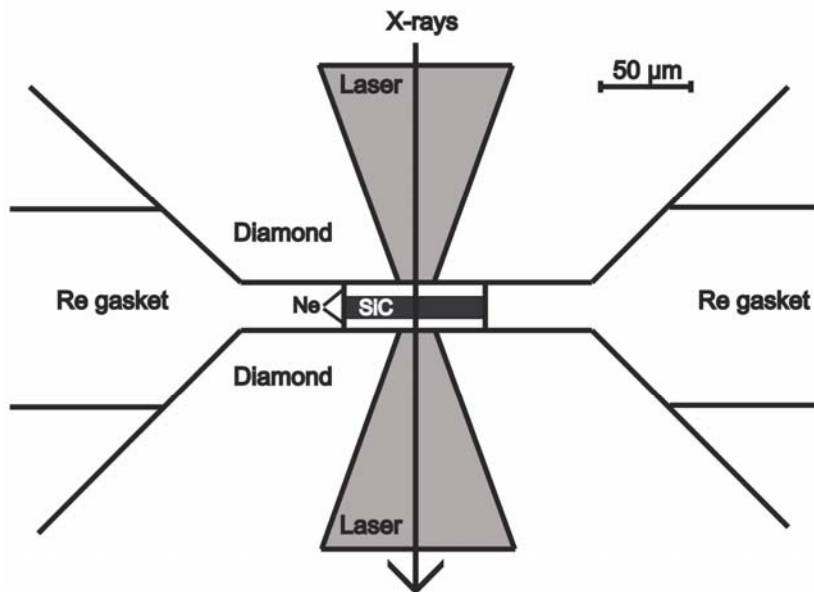


FIG 2.

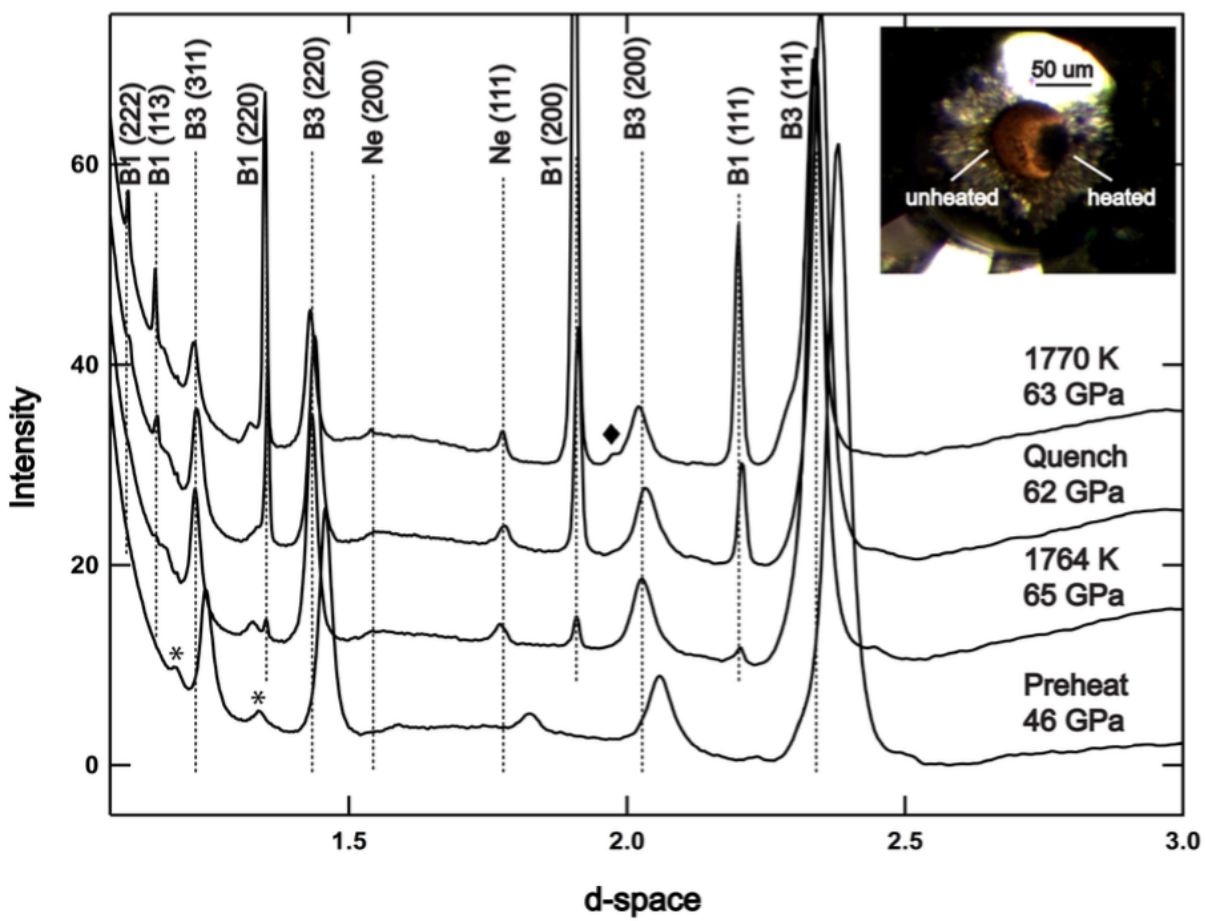


FIG. 3

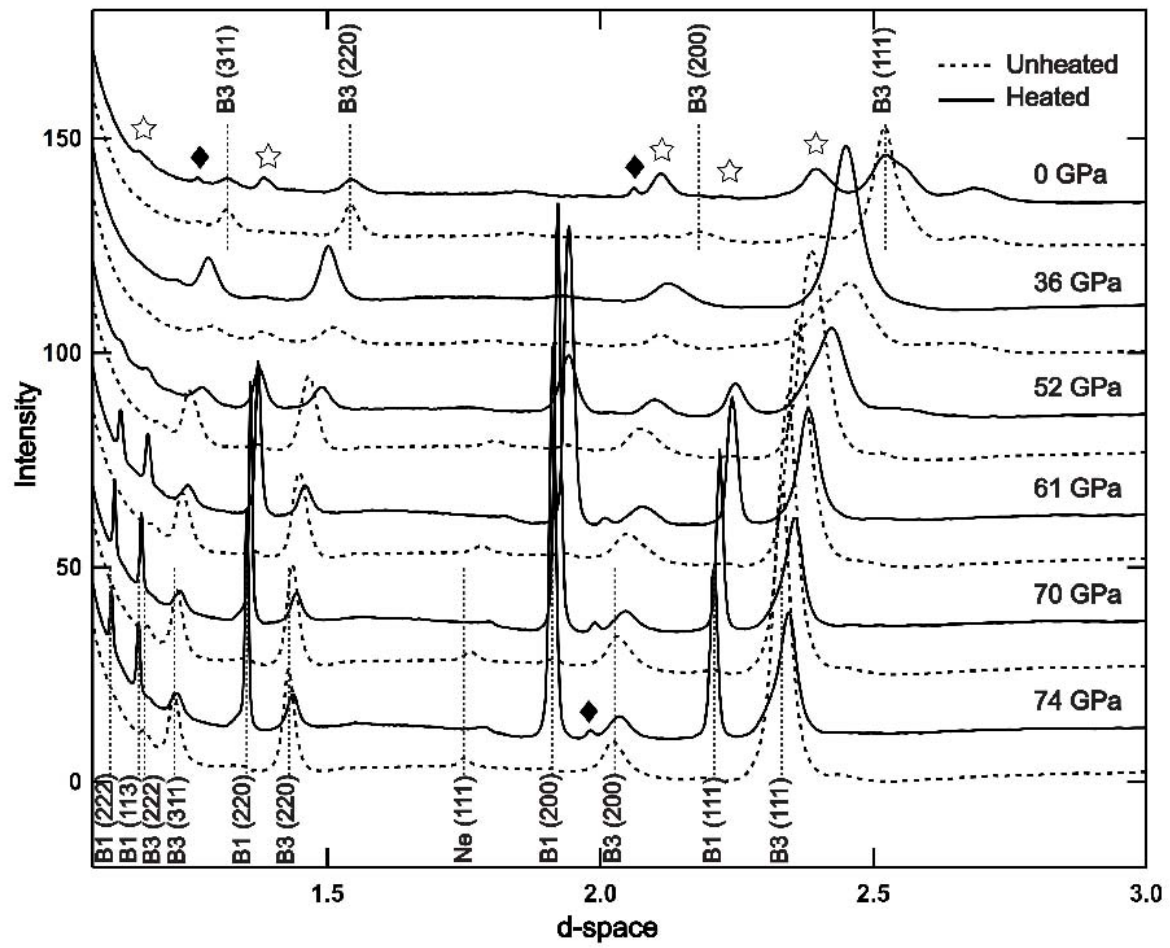


FIG 4.

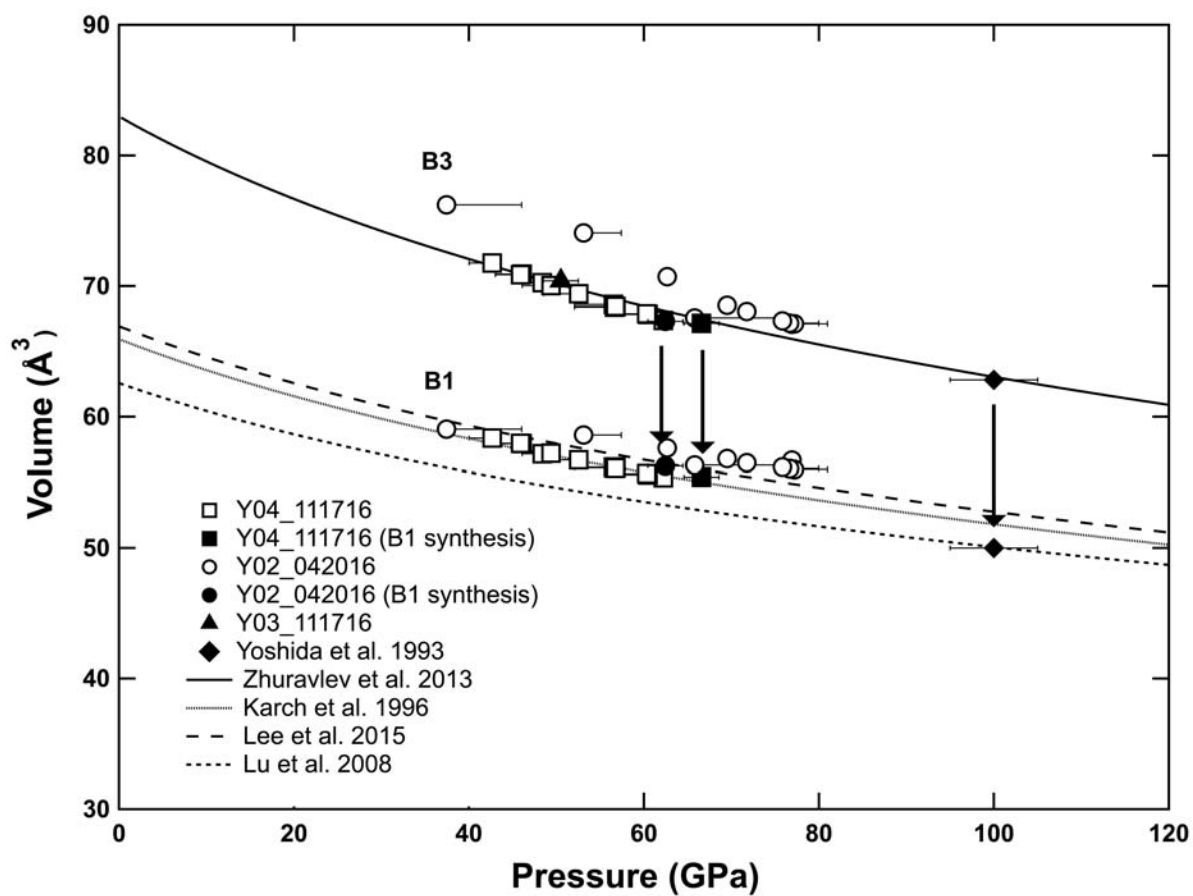


FIG 5.

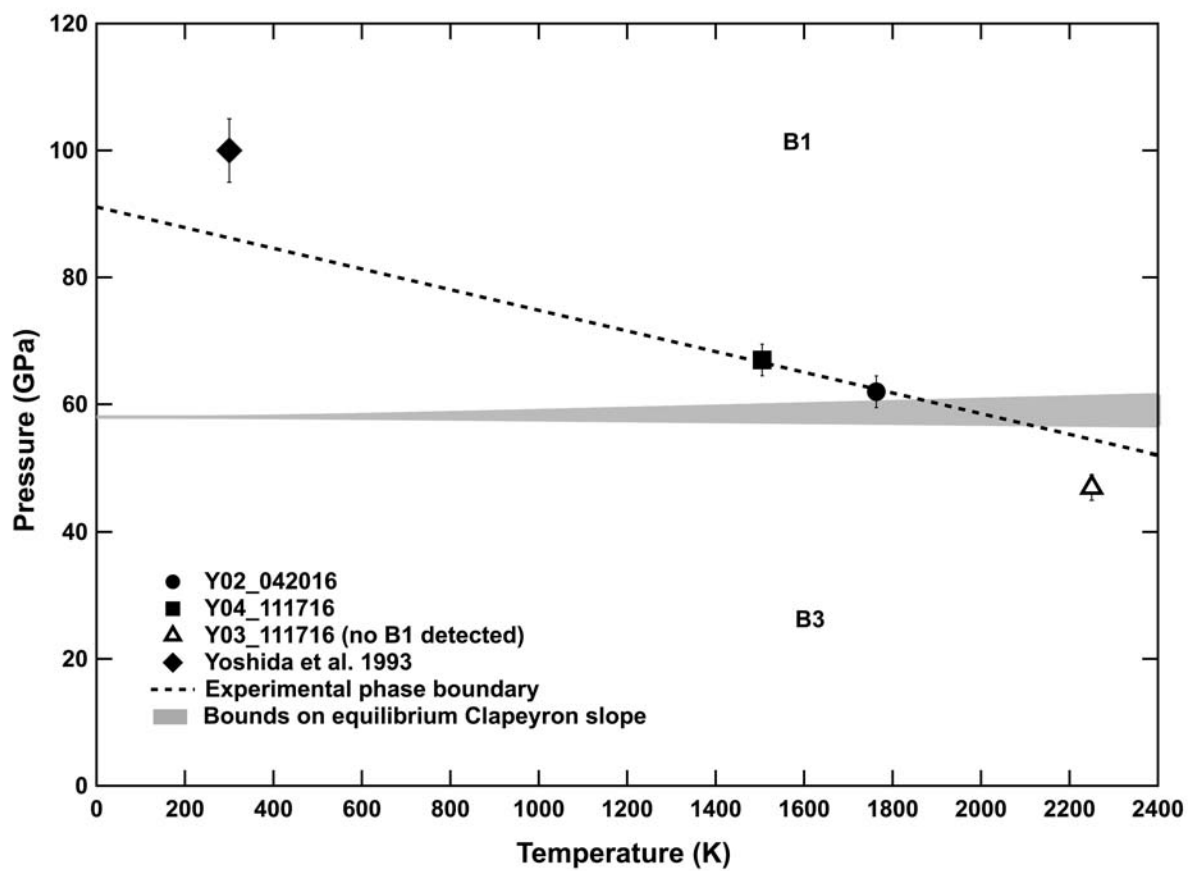


FIG 6

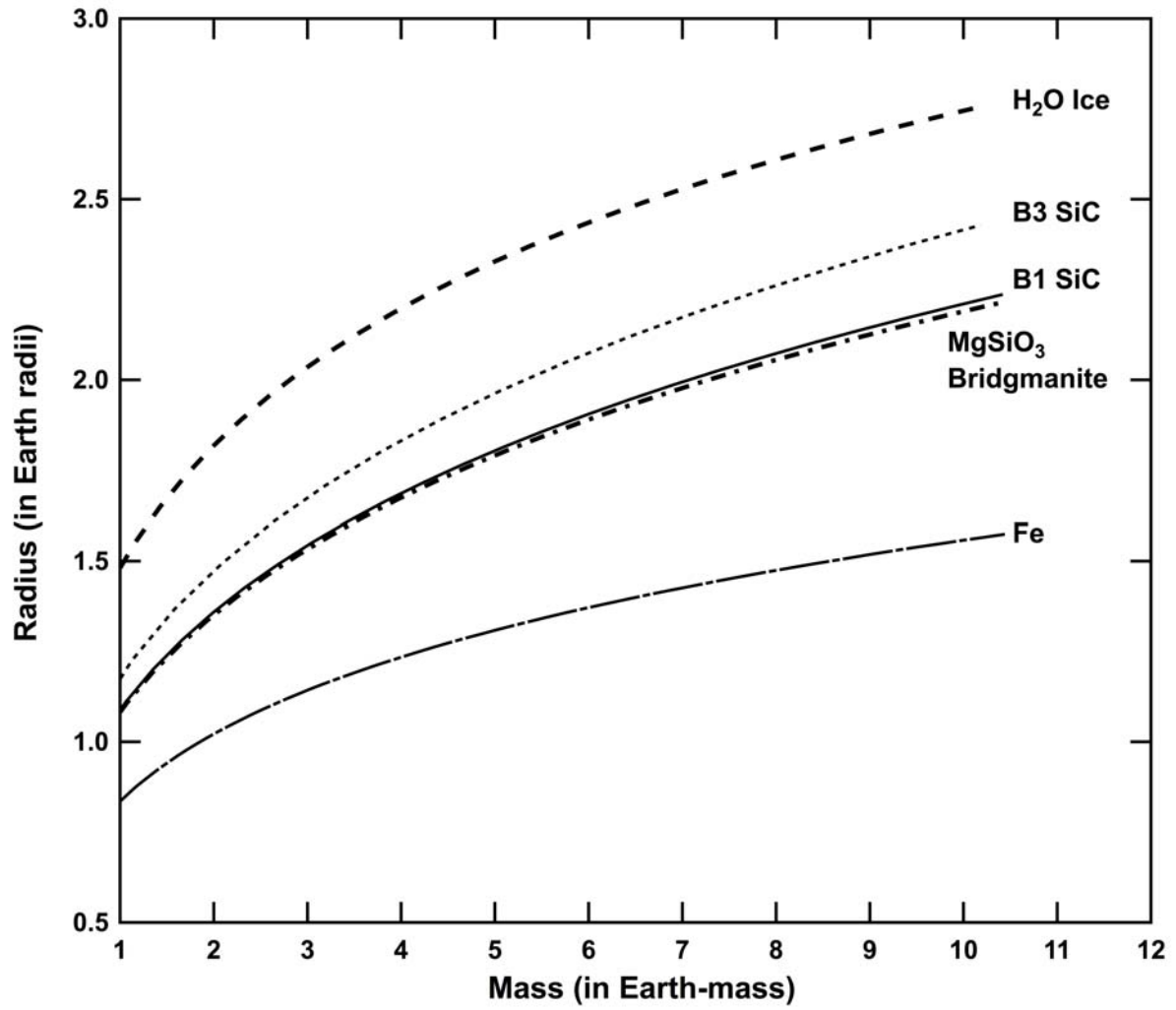


TABLE I. Experimental runs and conditions. Each sample was laser heated from two sides: up- and down-stream. The temperature listed first is the up-stream measurement, while the down-stream measurement is listed in parentheses. In order to maintain even heating, the temperatures between each side were kept to within  $\sim 100$  K of each other.

Experiment Name	Pressure before heating (GPa)	Pressure at B1 formation (GPa)	Temperature of B1 Appearance (K)	Peak Temperature (K)
Y02_042016	47	62.4	1763 (1765)	
Y04_111716	67	66.6	1505 (1481)	
Y03_111716	50	N/A	N/A	2250 (2265)*

\* Ne pressure of  $\sim 47$  GPa at peak temperature

TABLE II. Experimental d-spacings and intensities observed for rock-salt (B1) SiC at room temperatures.

This study; Y02_042016 (62.4 GPa)					100 GPa <sup>11</sup>			
Observed d-space	Observed Intensity	Calculated d-space	Calculated Intensity	Lattice Parameter ( $\text{\AA}$ )	hkl	d-space	Intensity	Lattice Parameter ( $\text{\AA}$ )
2.2112	37	2.2121	52	3.831 ( $\pm 0.001$ )	111	2.1288	22	3.684 ( $\pm 0.001$ )
1.9153	100	1.9157	100		200	1.8398	100	
1.3551	56	1.3546	85		220	1.3028	28	
1.1559	9	1.1552	44		113	-	-	
1.1074	6	1.1060	74		222	-	-	
This study; Y04_111716 (66.6 GPa)								
1.9068	100	1.9061	100		200			
1.3474	56	1.3478	85	3.812	220			
1.1492	16	1.1494	44	( $\pm 0.001$ )	113			
1.1001	12	1.1005	74		222			

<sup>11</sup>Reference [11]

TABLE III. Transition parameters for B3 to B1 transition as found by previous experiments and calculations.  $V_t/V_0$  represents the ratio of the volume of B1 at the transition pressure, to that of the room-pressure volume of B3.  $\Delta V(\%)$  shows the change in volume between B1 and B3 at the transition pressure.

Pressure (GPa)	$V_t/V_0$	$\Delta V(\%)$	Method	Reference
Experiments				
62.4	0.811	16.5	LHDAC	This Study
66.6	0.809	17.4	LHDAC	This Study
100	0.757	20.3	DAC	[11]
Computations				
58	0.825	18.1	DFT (PBE)	[6]
67	0.811	18.2	DFT (PBEsol)	
75.4	0.799	18	DFT (LDA)	[7]
63	0.80	18	DFT (GGA)	[8]
140	0.78	21	MD	[9]
66	0.819	17.9	DFT (LDA)	[5]
66	0.81	18.5	<i>Ab initio</i> pseudopotential	[3]